Author Manuscript

Author Manuscript

Author Manuscript

Author Manuscript

HHS Public Access

Author manuscript

Dev Dyn. Author manuscript; available in PMC 2019 May 01.

Published in final edited form as:

Dev Dyn. 2018 May ; 247(5): 741–753. doi:10.1002/dvdy.24624.

POSTNATAL DEVELOPMENT OF LYMPHATIC VASCULATURE IN THE BRAIN MENINGES

Rebecca M. Izen[*], **Tomoko Yamazaki**[*,#], **Yoko Nishinaka-Arai**[*,§], **Young-Kwon Hong**[¶], and **Yoh-suke Mukouyama**[*,†]

[*]Laboratory of Stem Cell and Neuro-Vascular Biology, Genetics and Developmental Biology Center, National Heart, Lung, and Blood Institute, National Institutes of Health, Building 10/6C103, 10 Center Drive, Bethesda, MD 20892, USA

[§]Department of Clinical Application, Center for iPS Cell Research and Application, Kyoto University, Kyoto 606-8507, Japan

[¶]Department of Surgery, Keck School of Medicine, University of Southern California, Los Angeles, CA90033

Abstract

Background—Traditionally, the central nervous system (CNS) has been viewed as an immune-privileged environment with no lymphatic vessels. This view was partially overturned by the discovery of lymphatic vessels in the dural membrane that surrounds the brain, in contact with the interior surface of the skull. We here examine the distribution and developmental timing of these lymphatic vessels.

Results—Using the *Prox1-GFP BAC* transgenic reporter and immunostaining with antibodies to lymphatic markers LYVE-1, Prox1, and Podoplanin, we have carried out whole-mount imaging of dural lymphatic vasculature at postnatal stages. We have found that between birth – postnatal day 13 (P)13, lymphatic vessels extend alongside dural blood vessels from the side of the skull towards the midline. Between P13 – P20, lymphatic vessels along the transverse sinuses (TS) reach the superior sagittal sinus (SSS) and extend along the SSS towards the olfactory bulb.

Conclusion—Compared with the embryonic developmental timing of lymphatic vessels in other tissues, e.g. skin, dural lymphatic vessel development is dramatically delayed. This study provides useful anatomical data for continuing investigations of the fundamental mechanisms that underlie dural lymphatic vessel development.

Keywords

Lymphatic vessels; Meningeal lymphatics; Prox1; Dura mater

[†]Author for correspondence: Tel: (301) 451-1663, FAX: (301) 480-1581, mukoyamay@mail.nih.gov.
[#]Current Address: Earle A. Chiles Research Institute, Robert W. Franz Cancer Center, Providence Portland Medical Center, Portland, OR 97213, USA

AUTHORS CONTRIBUTIONS

R.I. designed and performed most of the experiments and wrote the manuscript. T.Y. performed some experiments, provided experimental procedures, and wrote the manuscript. Y.N-A. performed some experiments. Y.K.H. provided essential reagents and experimental procedures. Y.M. directed this study and wrote the manuscript.

Author Manuscript Author Manuscript Author Manuscript Author Manuscript

INTRODUCTION

The central nervous system (CNS) has traditionally been viewed as an immune-privileged tissue, where adaptive immunity and inflammation are highly controlled. In seminal experiments, Medawar suggested that the absence of a lymphatic drainage system in the CNS may contribute to the brain's tolerance to foreign tissue grafts (Medawar, 1948). This view of the CNS as an immune-privileged site was partially overturned by the discovery of functional lymphatic vessels in the dural meningeal membrane, the outermost of three connective tissue layers (pia mater, arachnoid mater, and dura mater), that surround the brain (Aspelund et al., 2015; Louveau et al., 2015). The subarachnoid space between the dura mater and the inner meningeal layers is filled with cerebrospinal fluid (CSF), providing an interface between dural lymphatic vessels and the macromolecules and immune cells of the CNS. It is known that the dural lymphatics drain CSF, macromolecules, and immune cells from the CNS to the deep cervical lymph nodes (Aspelund et al., 2015; Louveau et al., 2015). However, most properties of these novel lymphatic vessels remain entirely unknown, including their developmental ontogeny.

The lymphatic system maintains tissue homeostasis by draining fluid from extracellular spaces back into the venous circulation (Reviewed in (Tammela and Alitalo, 2010). The lymph fluid is filtered through a series of lymph nodes, where foreign antigens from the extracellular spaces activate T- and B- cells to induce an immune response (Reviewed in (Bechmann and Woodroofe, 2014). Lymphatic development begins in the cardinal vein at embryonic day (E)9.5 – E10.5, when a subset of venous endothelial cells (ECs) express the transcription factor Prox1, the master regulator of lymphatic endothelial cell (LEC) fate (Wigle and Oliver, 1999). These Prox1-positive LECs bud off from the vein to form primordial lymphatic structures (Francois et al., 2012; Yang et al., 2012). Subsequent sprouting from aggregates of LECs is driven by vascular endothelial growth factor C (VEGF-C) and its receptor VEGF receptor 3 (VEGFR-3) (Dumont et al., 1998; Makinen et al., 2001; Karkkainen et al., 2004). The sprouting lymphatic vessels invade the skin and most internal organs within the embryo, covering tissues with a highly branched network of lymphatic vasculature (Sabin, 1902; Sabin, 1904; Makinen et al., 2007; Oliver and Srinivasan, 2008). Recent studies have revealed a surprising diversity in the origin and developmental timing of lymphatic vessels, which are adapted to the complex physiologies of different tissues such as heart (Klotz et al., 2015), skin (Martinez-Corral et al., 2015), intestine (Mahadevan et al., 2014), mesentery (Stanczuk et al., 2015), lymph node (Lee and Koh, 2016), and Schlemm's canal in eye (Aspelund et al., 2014; Park et al., 2014). In the CNS, further anatomical studies characterizing the three-dimensional architecture and development of meningeal lymphatics are required to better understand the meningeal lymphatic drainage. Here, we have investigated meningeal lymphatic development. We used the *Prox1-GFP BAC* transgenic reporter (Choi et al., 2011) and immunostaining with antibodies to lymphatic and blood EC markers. By confocal microscopy, we imaged large swaths of the inner surface of the skull, which is fused to the dural membrane and its meningeal blood and lymphatic vasculature. We found that the dural lymphatic vessels develop postnatally. Compared to other tissues, i.e skin where lymphatic vasculature develops from E13.5 onward, this is a dramatic developmental delay. Our comprehensive

Author Manuscript Author Manuscript Author Manuscript Author Manuscript

whole-mount imaging method provides useful anatomical data for continued investigations of the ontogeny of meningeal LECs and the molecular mechanisms underlying meningeal lymphatic vessel development.

RESULTS

High-resolution whole-mount imaging of adult meningeal lymphatics

We characterized the distribution of lymphatic vessels surrounding the adult brain using the *Prox1-GFP BAC* transgenic reporter (Choi et al., 2011). We carried out whole-mount immunohistochemical analysis of coronal skull sections over the SSS with antibodies to GFP together with the LEC marker LYVE-1 and pan-EC marker PECAM-1 (Fig. 1A). Prox1-GFP/LYVE-1-double positive lymphatic vessels were observed in contact with the interior surface of the skull (Fig. 1B and C), but not in the brain parenchyma (data not shown).

To visualize the meningeal lymphatic vessel network, we then developed a whole-mount skull dissection and antibody labelling protocol (Fig. 1A and D; Fig. 9A–D). Confocal tile scanning enabled us to image a large field of the inner surface (meningeal layers) of the dissected skull at high resolution (Fig. 1D–G). As described previously (Aspelund et al., 2015; Louveau et al., 2015), we found Prox1-GFP/LYVE-1-double positive lymphatic vessels adjacent to veins in the transverse sinus (TS) and superior sagittal sinus (SSS) in the meninges (Fig. 1E–F). These lymphatics appeared not to branch out from the sinus, indicative of a close anatomical relationship between meningeal lymphatics and the veins. Along the SSS, some of the lymphatic vessels appeared to be discontinuous. We also found Prox1-GFP-positive/LYVE-1-weak lymphatic vessels adjacent to a distal branch of the middle meningeal artery (MMA) (Fig. 1G, Aspelund et al., 2015). Combined, these experiments demonstrate that our whole-mount imaging technique allows us to visualize an anatomically recognizable pattern of the meningeal lymphatic network with a cellular resolution.

Whole-mount imaging of postnatal meningeal lymphatics

We next questioned how meningeal lymphatics develop in the postnatal period. To address this, we first examined formation of the meningeal lymphatic network at postnatal day (P)20. We used antibodies to GFP together with LYVE-1, Prox1, and Podoplanin as markers of lymphatic vessels. Prox1-GFP/LYVE-1-double positive lymphatic vessels were found adjacent to the TS and SSS, and lymphatic vessels also developed along a distal branch of MMA (Fig. 2A). The Prox1-GFP-positive lymphatic vessels were positive for Prox1 (Fig. 2B-B′, C-C′) and Podoplanin (Fig. 2D-D′). We observed labelling of a population of Prox1-GFP-positive non-lymphatic cells at the confluence of the sinuses (COS), which were not stained with antibodies to Prox1 and LYVE-1 and did not form a typical lymphatic network (Fig. 2A, E-E″). We clearly observed a small-diameter Prox1/PECAM-1-double positive lymphatic vessel (Fig. 2E-E″) and an extensive PECAM-1-positive blood vascular network (Fig. 2E and E″) at the confluence of the sinuses, suggesting that the lack of Prox1 and LYVE-1 immunostaining was not due to tissue damage or insufficient immunostaining. This is an unidentified, non-vascular cell population that may have temporally expressed the

Author Manuscript Author Manuscript Author Manuscript Author Manuscript

Prox1 protein, causing a perdurance of GFP. Prox1-GFP-negative/LYVE-1-positive individual cells were observed in close proximity to meningeal vasculature (Fig. 2A). These cells were positive for the macrophage markers F4/80 (Fig. 2F-F′) and CD206 (aka Mannose Receptor 1; Fig. 2G-G′), indicative of tissue-localized macrophages. The P20 meningeal lymphatic vasculature (Fig. 2A) had similar patterning to adult lymphatics (Fig. 1D), suggesting that the development had neared completion.

Meningeal lymphatic development at postnatal stages

To address when meningeal lymphatics emerge along the venous sinuses and the MMA, we analyzed a time-course of meningeal lymphatic development based on immunostaining with antibodies to lymphatic markers Prox1-GFP and LYVE-1. Initially, we focused our analysis on the top of the skull.

Established meningeal blood vascular networks, including the TS, SSS, and MMA, were observed along the top of the skull at P6 (Fig. 3A and D). The meningeal blood vasculature appeared to be established by P0 (data not shown). By P6, Prox1-GFP-negative/LYVE-1-positive individual cells (tissue-localized macrophages) had invaded the meninges and were mainly associated with the sinuses. The distribution of these macrophages was also established by P0 (data not shown). The lymphatic vascular network in ear skin was already well-established at P6 (Fig 3I-I″), but no lymphatics were observed in the meninges (Fig. 3A and D). By P13, Prox1-GFP/LYVE-1-double positive lymphatic vessels were detectable along the TS (Fig. 3B and E). By P16, Prox1-GFP/LYVE-1-double positive lymphatic vessels had extended along the TS to reach the SSS (Fig. 3C and F). Immunostaining with antibodies to GFP together with Prox1 and Podoplanin demonstrated that developing Prox1-GFP-positive lymphatic vessels and cell clusters were positive for Prox1 (Fig. 3G-G′) and Podoplanin (Fig. 3H-H′). Taken together with P20 data (Fig. 2), these results suggest that meningeal lymphatics develop during postnatal stages and extend along the TS, SSS, and MMA.

Overall, the lymphatic vessels developing adjacent to the TS and the MMA at top of the skull extended from the edges towards the midline. To examine lymphatic vessel development on the side of the skull, we modified our whole-mount skull dissection (Fig. 9E–I) and analysed a time-course of lymphatic development along the MMA (Fig. 4A) and TS (Fig. 5A and 6A). The MMA appeared to be established by P6, and Prox1-GFP-positive/LYVE-1-weak lymphatic vessels were associated with the MMA. (Fig. 4B). The lymphatic vessels at the base of the MMA connected with lymphatic vessels lining the pterygopalatine artery (PPA, Fig. 4B), which exits through foramina at the base of the skull. By P9, the Prox1-GFP-positive/LYVE-1-weak vessels extended along the MMA towards the top of the skull (Fig. 4C). By P20, Prox1-GFP-positive lymphatic vessels had extended along several branches of the MMA (Fig. 4D). We should note that the expression of LYVE-1 was enhanced in a subset of these Prox1-GFP-positive lymphatic vessels. The PPA-associated lymphatic vessels were Prox1-GFP/LYVE-1-double positive at every stage examined here. At P20, most lymphatic vessels along the MMA were Prox1-GFP/LYVE-1-double positive. (Fig. 4B–D). The Prox1-GFP-positive lymphatic vessels along the MMA and PPA were also

Author Manuscript Author Manuscript Author Manuscript Author Manuscript

positive for Prox1 (Fig. 4E–F′) and Podoplanin (Fig. 4G–H′). Taken together, these results indicate that lymphatic vessels lining the MMA extend from the base of the skull.

Along the side of the skull, the TS runs from the SSS to the ear, where it connects to the retroglenoid vein (RGV) and sigmoid sinus (SS) (Fig. 5A). We imaged a large field of the side of the skull to identify whether lymphatic vessels on the TS are extensions of lymphatic vessels along the RGV and SS (Fig. 5B). The RGV is slightly rostral to the TS, and it extends approximately in parallel from the TS to the base of the skull. The SS is caudal to the TS and branches around the ear, initially perpendicular to the TS. Both the RGV and the SS exit through foramina at the base of the skull. At P11, we observed Prox1-GFP-positive/LYVE-1-weak lymphatic vessels along the SS extending towards the base of the TS (Fig. 5B). The RGV region between the TS and the base of the skull appeared to be devoid of lymphatic vessels. Due to technical issues, however, we could not define a connection between the TS and the large-diameter RGV. Therefore, we focused our studies on the route of lymphatic vessel extension from the SS to the TS. Developing Prox1-GFP-positive lymphatic vessels and cell clusters at the base of the TS were also positive for Prox1 (Fig. 5C-C′) and Podoplanin (Fig. 5D-D′). From P11–P20, lymphatic vessels along the TS extended towards the top of the skull, and lymphatic vessels along the SS extended upwards to connect with the TS lymphatic vessels (Fig. 6B–D). A subset of the Prox1-GFP-positive lymphatic vessels along the TS and SS showed enhanced LYVE-1 expression at P13 (Fig. 6C) and P20 (Fig. 6D). Overall, these results indicate that the lymphatic vessels observed along the TS at the top of the skull were coming from the TS and SS along the side of the skull. The SS may be a possible route for lymphatic vessels to enter through foramina at the base of the skull. Whether lymphatic vessels grow along the RGV remains to be investigated.

We next examined where meningeal lymphatics emerge. To address this, we focused our studies on the base of the MMA at P0. We developed a whole-mount skull dissection to image lymphatic and blood vasculature at the base of the skull (Fig. 7A; Fig. 9J–P). A Prox1-GFP-positive vascular plexus was observed surrounding the base of the MMA (Fig. 7B). A subset of the vascular plexus was positive for Prox1 (Fig. 7C–C′) and Podoplanin (Fig. 7D-D′). These data suggest that lymphatics emerge along the base of the MMA. Interestingly, the majority of the PECAM-1-positive vascular plexus surrounding the MMA was positive for Prox1-GFP (Fig. 7B, C-C′. D-D′) but negative for Prox1 (Fig. 7C-C′) and Podoplanin (Fig. 7D-D′). This result suggests that a perdurance of GFP was detected in these PECAM-1-positive ECs after Prox1 down-regulation. Moreover, the perdurance of GFP was detectable in a subset of EMCN-positive venous and capillary ECs (Fig. 7E-E′). Further experiments are needed to determine whether these Prox1-GFP-positive/Prox1-negative venous and capillary ECs differentiate into LECs at the base of the skull.

DISCUSSION

We here report our extensive whole-mount imaging of meningeal lymphatic vessels in contact with the adult and postnatal skull. Our data suggest that meningeal lymphatic vessels extend from the base of the skull to the midline of the skull (Fig. 8A–B). Between P0–P20, lymphatic vessels extend from the base of the TS and MMA to reach the top of the skull

Author Manuscript Author Manuscript Author Manuscript Author Manuscript

(Fig. 8A). Between P13–P20, lymphatic vessels extend along the TS to reach the SSS (Fig. 8B). The lymphatic vessels then extend along the SSS towards the olfactory bulb (Fig. 8B). By P20, the meningeal lymphatic vessel extension appears to have neared completion.

Compared to lymphatic vessel development in other tissues, e.g. skin where lymphatic vasculature develops from E13.5 onward, the meningeal lymphatics develop at a delayed developmental time point. One possible explanation is that this delay may correspond to the developmental timing of the meninges and skull. The meninges originate from mesenchymal and encephalic neural crest cells (Decimo et al., 2012). The three meningeal layers are formed from a single pial meshwork structure after the neural tube closure. By E14.5 three primitive meningeal layers, including the pia mater with blood vessels, develop between the brain and the frontal bone domain (Vivatbutsiri et al., 2008). Interestingly, we found major venous sinuses (TS and SSS) surrounding the E14.5 brain, but no significant lymphatics were observed (data not shown). The mineralization of skull bones within the skeltogenic membrane, which is located between the dermal mesenchyme and the meninges surrounding the brain, is initiated in the frontal and parietal bones around E16.5 (Iseki et al., 1997). By E18.5, the mineralization has extended apically to the top of the head (Iseki et al., 1997). In the postnatal stage, the dura mater provides osteogenic signals and extracellular matrix which support the calvarial bone formation (Vivatbutsiri et al., 2008). This postnatal interaction between the meninges and skull development may trigger the recruitment of lymphatic vessels into the dural meningeal layer.

A very recent work reported by the Alitalo group is consistent with our observation that meningeal lymphatic vessels develop postnatally, appearing first at the base of the skull (Antila et al., 2017). Their work also found that VEGF-C is highly expressed by vascular smooth muscle cells that cover meningeal blood vessels and that VEGF-C-VEGFR3 signaling is essential for the meningeal lymphatic development. However, the developmental origin of meningeal LECs remains unclear. Emerging studies have highlighted the heterogeneous origins of LECs in an organ-specific manner (Reviewed in (Kazenwadel and Harvey, 2016; Semo et al., 2016) In the meninges, one population of LECs may develop via extension of lymphatic vessels from other tissues into the brain meninges. The SS is one possible route for lymphatic vessels to enter the meninges through foramina at the base of the skull. An additional population of meningeal LECs may originate from meningeal blood endothelial cells (BECs) and/or meningeal non-vascular cells, i.e. LYVE-1-positive macrophages. A local origin of LECs was recently observed in Schlemm’s canal, a specialized lymphatic vasculature in the eye. Schlemm’s canal originates from the local blood vasculature at postnatal stages when initial endothelial buds from choroidal veins acquire lymphatic character (Aspelund et al., 2014; Park et al., 2014). Similarly, we found a Prox1-GFP-positive blood vascular network at the base of the skull as well as Prox1-GFP/Prox1/Podolanin-triple positive lymphatic sprouts along the MMA. We should note that the subset of venous and capillary ECs which are positive for Prox1-GFP but negative for Prox1 protein and Podoplanin could reflect the perdurance of GFP after Prox1 down-regulation. It is not clear whether such temporal expression of Prox1 corresponds to the differentiation potential of venous and capillary ECs into LECs. To further address the developmental origin of meningeal lymphatics, extensive lineage tracing experiments using inducible BEC- and LEC-specific *CreER* drivers should be carried out.

Author Manuscript Author Manuscript Author Manuscript Author Manuscript

We have observed that Prox1-GFP-negative/LYVE-1-positive individual cells are distributed in close proximity to meningeal vasculature and express the macrophage markers CD206 and F4/80, indicative of tissue-localized macrophages. Interestingly, LYVE-1-positive perivascular cells with macrophage-like morphology have also been reported on the surface of the zebrafish brain (Bower et al., 2017; Venero Galanternik et al., 2017). These cells express Prox1, but no other macrophage markers, and are not of hematopoietic origin. Rather, they are derived from BECs within the brain. Further characterization using lineage tracing experiments are needed to compare zebrafish LYVE-1-positive perivascular cells with murine Prox1-GFP-negative/LYVE-1-positive cells in the meningeal vasculature.

EXPERIMENTAL PROCEDURES

Experimental Animals

The characterization of *Prox1-GFP BAC* transgenic mice (Choi et al., 2011) has been reported elsewhere. All experiments were carried out according to the guidelines approved by the National Heart, Lung, and Blood Institute Animal Care and Use Committee.

Whole-mount Immunostaining of the Brain Meninges

Postnatal and adult skull dissections (Fig. 9) were adapted from (Aspelund et al., 2015). After dissection, skulls and their attached meningeal membranes were fixed in 4% paraformaldehyde (PFA)/phosphate-buffered saline (PBS) at 4°C overnight and washed in ice-cold PBS. Skulls were decalcified using 0.5M EDTA, pH 7.4, at 4°C overnight. Skulls were blocked in 10% Heat-inactivated Goat Serum (HIGS)/PBS + 0.5% Triton X-100 (TX100) for one hour and stained with primary antibodies (see Table 1) at 4°C overnight with rotation. Skulls were washed in 2% HIGS/PBS + 0.5% TX100 five times at 15-minute intervals with nutation. Skulls were stained with secondary antibodies at 4°C overnight with rotation. Different combinations of Alexa Fluor-488-, Alexa Fluor-568-, Cy3- or Alexa Fluor-647-conjugated secondary antibodies (Invitrogen/Thermo Fisher Scientific 1:300 or Jackson Immunoresearch, 1:300) were used for different staining. Skulls were washed in 2% HIGS/PBS + 0.5% TX100 five times at 15-minute intervals with nutation and stored in PBS at 4°C prior to imaging. Skulls were mounted with Prolong Gold (Thermo Fisher Scientific) in 0.5mm spacers (Life Technologies/Thermo Fisher Scientific) and imaged immediately using a Leica TCS SP5 confocal microscope. To observe Prox1 nuclear staining, the skull sample needed to be in direct contact with the cover slip. Since the skull has a three-dimensional structure, this was not possible using a 0.5mm spacer. In lieu of a spacer, two 25mm x 25mm cover slips (Thermo Fisher Scientific) were superglued to the slide glass. The skull sample was mounted in Prolong Gold, and a third cover slip was superglued over the sample.

Section Immunostaining of the Brain Meninges

Adult mice were fixed by cardiac perfusion. The entire skull and attached meningeal membrane, with the brain still inside, was post-fixed in 4% PFA/PBS overnight and washed with ice-cold PBS. The brain/skull samples were decalcified in 0.5M EDTA, pH 7.4, at 4°C for one week. Samples were washed with ice-cold PBS and incubated in a 30% Sucrose/PBS solution for one week prior to embedding in OCT compound (Tissue Tech). Samples were

Author Manuscript Author Manuscript Author Manuscript Author Manuscript

sectioned into 60 μm sections using a Leica CM1900 cryostat. Staining was performed similarly to above, but with no nutation or rotation. Sections were mounted with Prolong Gold (Thermo Fisher Scientific) and dried overnight prior to imaging with a Leica TCS SP5 confocal microscope.

Whole-mount Immunostaining of Skin

Whole-mount skin and tissue section staining was performed as previously described (Mukouyama et al., 2002; Li and Mukouyama, 2011; Yamazaki et al., 2018). All confocal microscopy was carried out on a Leica TCS SP5 confocal.

Acknowledgments

Grant support information: The Intramural Research Program of the National Heart, Lung, and Blood Institute, NIH (HL005702-11 to Y.M.)

We thank J. Hawkins and the staff of NIH Bldg50 animal facility for assistance with mouse breeding and care, K. Gill for laboratory management and technical support, and R. Reed and F. Baldrey for administrative assistance. Thanks also to other members of Laboratory of Stem Cell and Neuro-Vascular Biology for technical help and thoughtful discussion. T. Yamazaki was supported by the Japan Society for the Promotion of Science (JSPS) NIH-KAITOKU. None of the authors have any financial or other conflicts of interest. This work was supported by the Intramural Research Program of the National Heart, Lung, and Blood Institute, National Institutes of Health (HL005702-11 to Y.M.).

References

Antila S, Karaman S, Nurmi H, Airavaara M, Voutilainen MH, Mathivet T, Chilov D, Li Z, Koppinen T, Park JH, Fang S, Aspelund A, Saarma M, Eichmann A, Thomas JL, Alitalo K. Development and plasticity of meningeal lymphatic vessels. J Exp Med. 2017; 214:3645–3667. [PubMed: 29141865]

Aspelund A, Antila S, Proulx ST, Karlsen TV, Karaman S, Detmar M, Wiig H, Alitalo K. A dural lymphatic vascular system that drains brain interstitial fluid and macromolecules. J Exp Med. 2015; 212:991–999. [PubMed: 26077718]

Aspelund A, Tammela T, Antila S, Nurmi H, Leppanen VM, Zarkada G, Stanczuk L, Francois M, Makinen T, Saharinen P, Immonen I, Alitalo K. The Schlemm's canal is a VEGF-C/VEGFR-3-responsive lymphatic-like vessel. J Clin Invest. 2014; 124:3975–3986. [PubMed: 25061878]

Bechmann, I., Woodroofe, N. Immune Privilege of the Brain. In: Woodroofe, N., Amor, S., editors. Neuroinflammation and CNS Disorders. John Wiley & Sons, Ltd; 2014. p. 1-8.

Bower NI, Koltowska K, Pichol-Thievend C, Virshup I, Paterson S, Lagendijk AK, Wang W, Lindsey BW, Bent SJ, Baek S, Rondon-Galeano M, Hurley DG, Mochizuki N, Simons C, Francois M, Wells CA, Kaslin J, Hogan BM. Mural lymphatic endothelial cells regulate meningeal angiogenesis in the zebrafish. Nat Neurosci. 2017; 20:774–783. [PubMed: 28459441]

Choi I, Chung HK, Ramu S, Lee HN, Kim KE, Lee S, Yoo J, Choi D, Lee YS, Aguilar B, Hong YK. Visualization of lymphatic vessels by Prox1-promoter directed GFP reporter in a bacterial artificial chromosome-based transgenic mouse. Blood. 2011; 117:362–365. [PubMed: 20962325]

Decimo I, Fumagalli G, Berton V, Krampera M, Bifari F. Meninges: from protective membrane to stem cell niche. Am J Stem Cells. 2012; 1:92–105. [PubMed: 23671802]

Dumont DJ, Jussila L, Taipale J, Lymboussaki A, Mustonen T, Pajusola K, Breitman M, Alitalo K. Cardiovascular failure in mouse embryos deficient in VEGF receptor-3. Science. 1998; 282:946–949. [PubMed: 9794766]

Francois M, Short K, Secker GA, Combes A, Schwarz Q, Davidson TL, Smyth I, Hong YK, Harvey NL, Koopman P. Segmental territories along the cardinal veins generate lymph sacs via a ballooning mechanism during embryonic lymphangiogenesis in mice. Developmental biology. 2012; 364:89–98. [PubMed: 22230615]

Author Manuscript Author Manuscript Author Manuscript Author Manuscript

Iseki S, Wilkie AO, Heath JK, Ishimaru T, Eto K, Morriss-Kay GM. Fgfr2 and osteopontin domains in the developing skull vault are mutually exclusive and can be altered by locally applied FGF2. Development. 1997; 124:3375–3384. [PubMed: 9310332]

Karkkainen MJ, Haiko P, Sainio K, Partanen J, Taipale J, Petrova TV, Jeltsch M, Jackson DG, Talikka M, Rauvala H, Betsholtz C, Alitalo K. Vascular endothelial growth factor C is required for sprouting of the first lymphatic vessels from embryonic veins. Nature Immunology. 2004; 5:74–80. [PubMed: 14634646]

Kazenwadel J, Harvey NL. Morphogenesis of the lymphatic vasculature: A focus on new progenitors and cellular mechanisms important for constructing lymphatic vessels. Dev Dyn. 2016; 245:209–219. [PubMed: 26228815]

Klotz L, Norman S, Vieira JM, Masters M, Rohling M, Dube KN, Bollini S, Matsuzaki F, Carr CA, Riley PR. Cardiac lymphatics are heterogeneous in origin and respond to injury. Nature. 2015; 522:62–67. [PubMed: 25992544]

Lee YG, Koh GY. Coordinated lymphangiogenesis is critical in lymph node development and maturation. Dev Dyn. 2016; 245:1189–1197. [PubMed: 27623309]

Li W, Mukouyama YS. Whole-mount immunohistochemical analysis for embryonic limb skin vasculature: a model system to study vascular branching morphogenesis in embryo. J Vis Exp. 2011

Louveau A, Smirnov I, Keyes TJ, Eccles JD, Rouhani SJ, Peske JD, Derecki NC, Castle D, Mandell JW, Lee KS, Harris TH, Kipnis J. Structural and functional features of central nervous system lymphatic vessels. Nature. 2015; 523:337–341. [PubMed: 26030524]

Mahadevan A, Welsh IC, Sivakumar A, Gludish DW, Shilvock AR, Noden DM, Huss D, Lansford R, Kurpios NA. The left-right Pitx2 pathway drives organ-specific arterial and lymphatic development in the intestine. Dev Cell. 2014; 31:690–706. [PubMed: 25482882]

Makinen T, Jussila L, Veikkola T, Karpanen T, Kettunen MI, Pulkkanen KJ, Kauppinen R, Jackson DG, Kubo H, Nishikawa S, Yla-Herttuala S, Alitalo K. Inhibition of lymphangiogenesis with resulting lymphedema in transgenic mice expressing soluble VEGF receptor-3. Nature medicine. 2001; 7:199–205.

Makinen T, Norrmen C, Petrova TV. Molecular mechanisms of lymphatic vascular development. Cell Mol Life Sci. 2007; 64:1915–1929. [PubMed: 17458498]

Martinez-Corral I, Ulvmar MH, Stanczuk L, Tatin F, Kizhatil K, John SW, Alitalo K, Ortega S, Makinen T. Nonvenous origin of dermal lymphatic vasculature. Circ Res. 2015; 116:1649–1654. [PubMed: 25737499]

Medawar PB. Immunity to homologous grafted skin; the fate of skin homografts transplanted to the brain, to subcutaneous tissue, and to the anterior chamber of the eye. Br J Exp Pathol. 1948; 29:58–69. [PubMed: 18865105]

Mukouyama YS, Shin D, Britsch S, Taniguchi M, Anderson DJ. Sensory nerves determine the pattern of arterial differentiation and blood vessel branching in the skin. Cell. 2002; 109:693–705. [PubMed: 12086669]

Oliver G, Srinivasan RS. Lymphatic vasculature development: current concepts. Ann N Y Acad Sci. 2008; 1131:75–81. [PubMed: 18519960]

Park DY, Lee J, Park I, Choi D, Lee S, Song S, Hwang Y, Hong KY, Nakaoka Y, Makinen T, Kim P, Alitalo K, Hong YK, Koh GY. Lymphatic regulator PROX1 determines Schlemm's canal integrity and identity. J Clin Invest. 2014; 124:3960–3974. [PubMed: 25061877]

Sabin FR. On the origin of the lymphatic system from the veins and the development of the lymph hearts and thoracic duct in the pig. Am J Anat. 1902:367–389.

Sabin FR. On the development of the superficial lymphatics in the skin of the pig. Am J Anat. 1904; 3:183–195.

Semo J, Nicenboim J, Yaniv K. Development of the lymphatic system: new questions and paradigms. Development. 2016; 143:924–935. [PubMed: 26980792]

Stanczuk L, Martinez-Corral I, Ulvmar MH, Zhang Y, Lavina B, Fruttiger M, Adams RH, Saur D, Betsholtz C, Ortega S, Alitalo K, Graupera M, Makinen T. cKit Lineage Hemogenic Endothelium-Derived Cells Contribute to Mesenteric Lymphatic Vessels. Cell Rep. 2015; 10:1708–1721.

Author Manuscript Author Manuscript Author Manuscript Author Manuscript

Tammela T, Alitalo K. Lymphangiogenesis: Molecular mechanisms and future promise. Cell. 2010; 140:460–476. [PubMed: 20178740]

Venero Galanternik M, Castranova D, Gore AV, Blewett NH, Jung HM, Stratman AN, Kirby MR, Iben J, Miller MF, Kawakami K, Maraia RJ, Weinstein BM. A novel perivascular cell population in the zebrafish brain. Elife. 2017:6.

Vivatbutsiri P, Ichinose S, Hytonen M, Sainio K, Eto K, Iseki S. Impaired meningeal development in association with apical expansion of calvarial bone osteogenesis in the Foxc1 mutant. J Anat. 2008; 212:603–611. [PubMed: 18422524]

Wigle JT, Oliver G. Prox1 function is required for the development of the murine lymphatic system. Cell. 1999; 98:769–778. [PubMed: 10499794]

Yamazaki T, Li W, Yang L, Li P, Cao H, Motegi SI, Udey MC, Bernhard E, Nakamura T, Mukouyama YS. Whole-Mount Adult Ear Skin Imaging Reveals Defective Neuro-Vascular Branching Morphogenesis in Obese and Type 2 Diabetic Mouse Models. Sci Rep. 2018; 8:430. [PubMed: 29323138]

Yang Y, Garcia-Verdugo JM, Soriano-Navarro M, Srinivasan RS, Scallan JP, Singh MK, Epstein JA, Oliver G. Lymphatic endothelial progenitors bud from the cardinal vein and intersomitic vessels in mammalian embryos. Blood. 2012; 120:2340–2348. [PubMed: 22859612]

Author Manuscript Author Manuscript Author Manuscript Author Manuscript

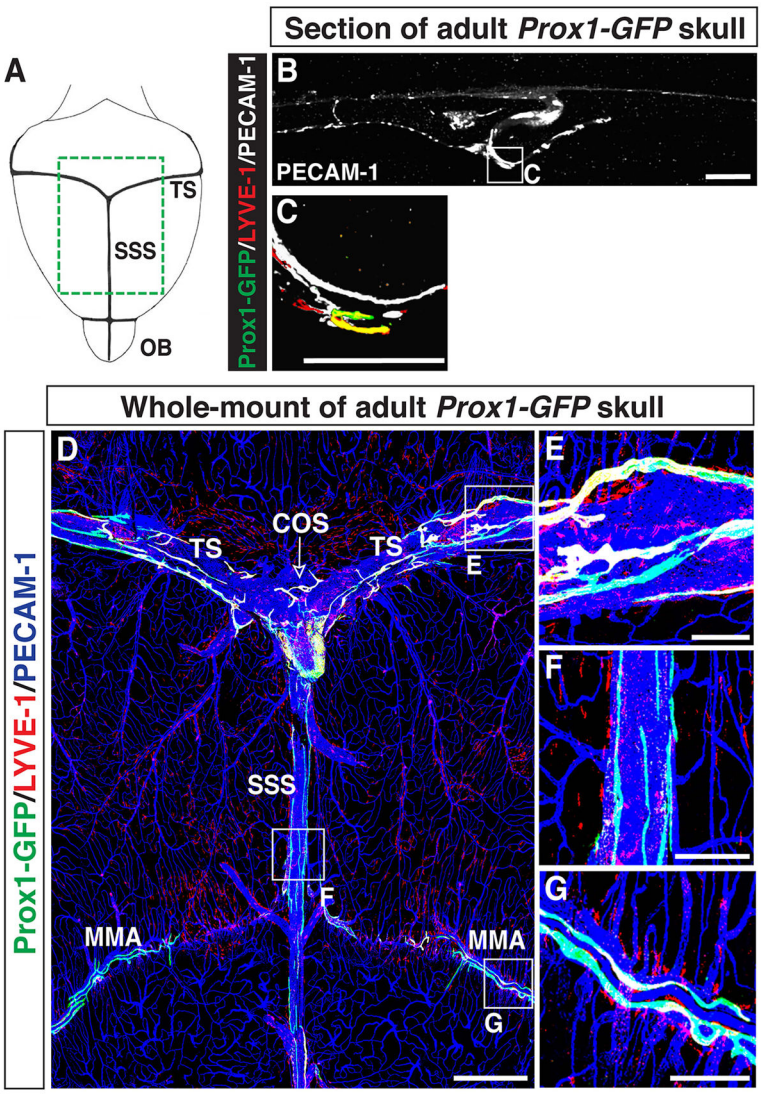

Figure 1.

Lymphatic vessels exist in the adult brain meninges. (A) The olfactory bulb (OB) and large diameter veins, i.e. the transverse sinus (TS) and the superior sagittal sinus (SSS), are viewed from the top of the brain/skull. The green area is displayed in (D). (B–C) Section staining of the adult skull over the SSS with antibodies to GFP together with lymphatic marker LYVE-1 and pan-endothelial cell marker PECAM-1. Prox1-GFP/LYVE-1/PECAM-1-triple positive lymphatic vessels are attached to the inside of the skull. The boxed region in (B) is magnified in (C). (D) Whole-mount staining of meninges attached to the inside of the skull in *Prox1-GFP* mice with antibodies to GFP, LYVE-1 and PECAM-1. Thin lymphatic vessels line the TS (E), the confluence of the sinuses (COS, open arrow), and the SSS (F) as well as the middle meningeal artery (MMA) (G). The boxed regions in (D) are magnified in (E–G). Scale = 100μm in (B–C, E–G) and 1mm in (D).

Author Manuscript Author Manuscript Author Manuscript Author Manuscript

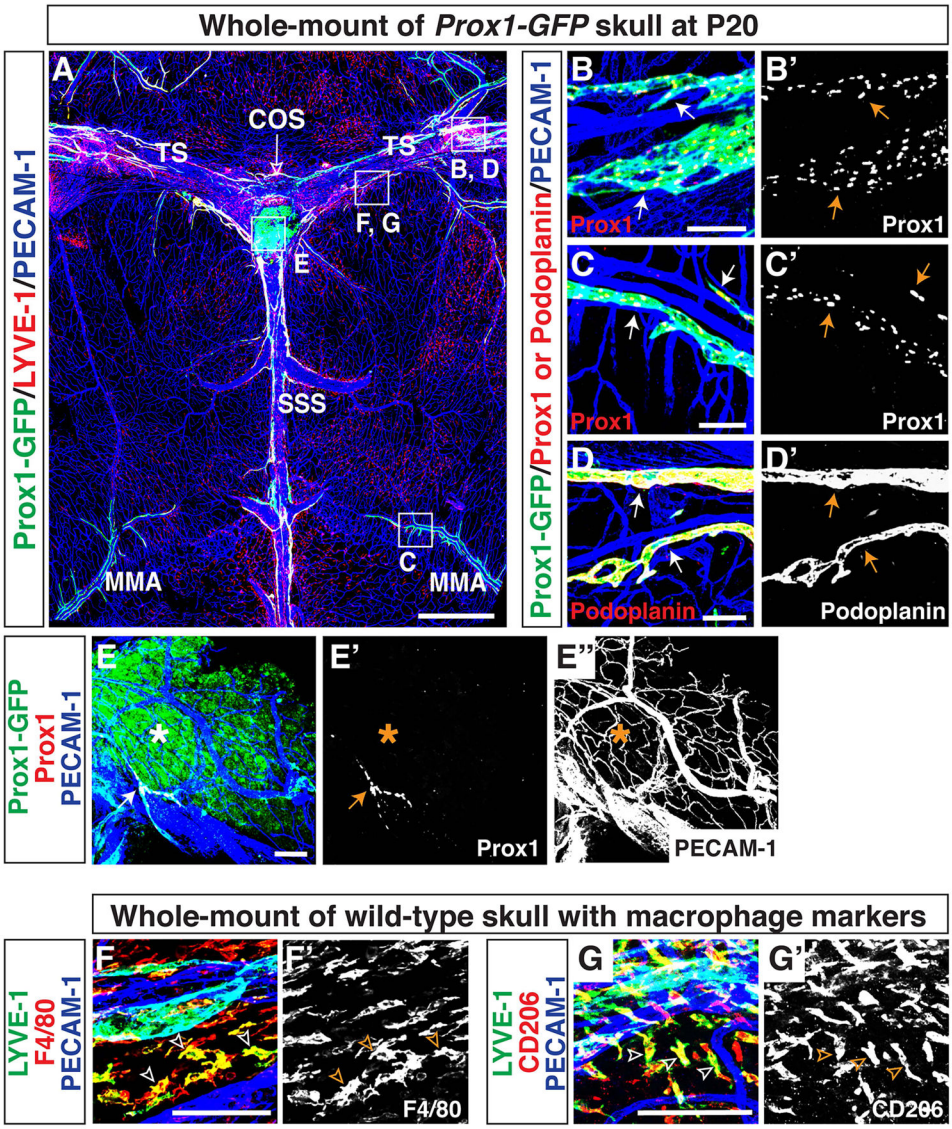

Figure 2.

Lymphatic vessels in the postnatal brain meninges express well-established lymphatic markers. (A) Lymphatic vessel patterning at postnatal day (P)20 is similar to the patterning in adult. In addition to lining the SSS, TS, COS (open arrow), and MMA, lymphatic vessels extend along additional smaller blood vessels in the meninges. The boxed regions in (A) are magnified in (B–G), with staining using different antibodies. (B-B′) Lymphatics along the TS are positive for both Prox1-GFP and Prox1 proteins (arrows). (C-C′) Lymphatics along the MMA are positive for both Prox1-GFP and Prox1 proteins (arrows). (D-D′) Lymphatic vessels along the TS are positive for lymphatic marker Podoplanin (arrows). (E-E″) The Prox1-GFP-positive area (asterisk) at the COS (open arrow) is not stained with anti-Prox1 antibody, indicating that this is not a real lymphatic region. Note that a small-diameter Prox1/PECAM-1-double positive lymphatic vessel (E and E′, arrow) and a PECAM-1-positive blood vascular network (E and E″) are observed at the COS. (E–F′) LYVE-1-positive cells in the meninges are also positive for the macrophage markers F4/80 (F-F′,

Author Manuscript Author Manuscript Author Manuscript Author Manuscript

open arrowheads) and CD206 (G-G′, open arrowheads) indicating that LYVE-1 single-positive cells in (A) are a subset of tissue macrophages. Scale = 1mm in (A) and 100 μm in (B–G, B′–G′).

Author Manuscript Author Manuscript Author Manuscript Author Manuscript

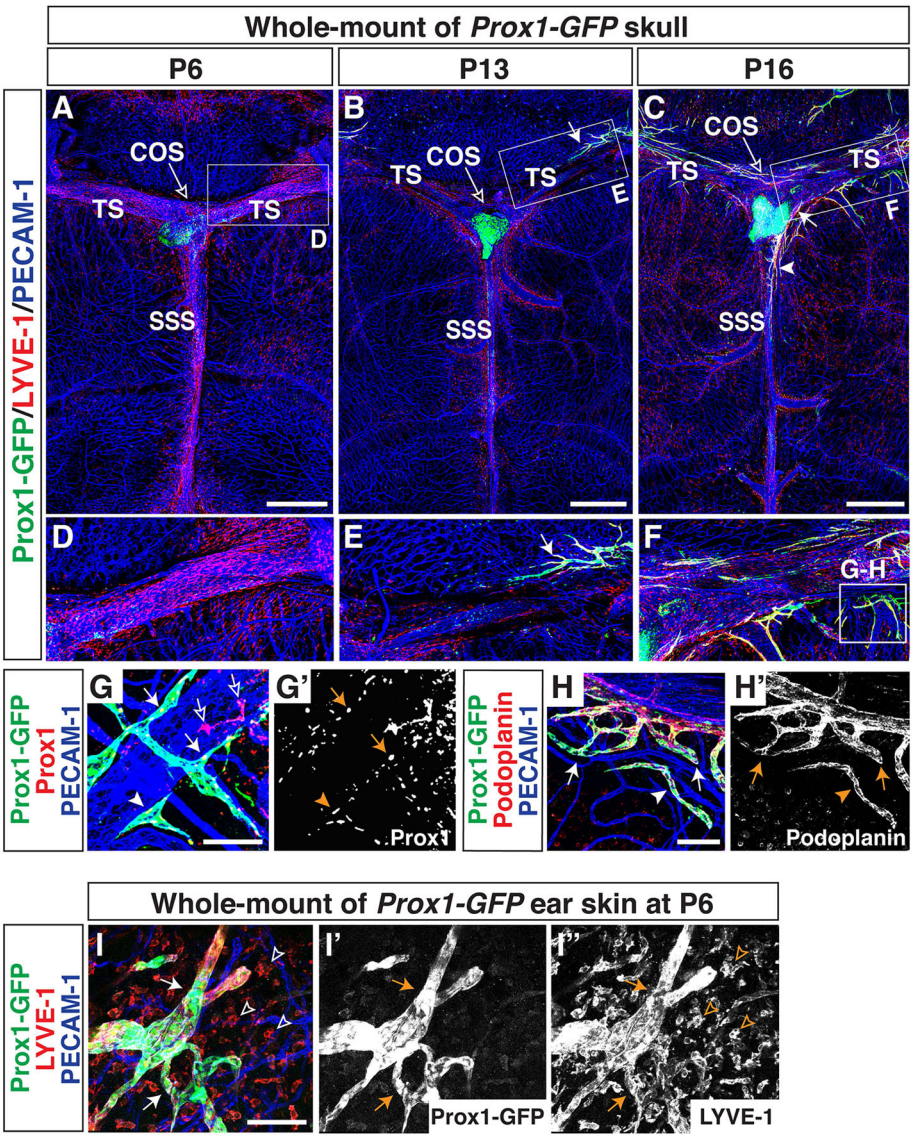

Figure 3.

Lymphatics develop at postnatal stages and extend along meningeal blood vessels from the side of the skull towards the midline. (A, D) At P6, lymphatics are not observed in the meninges at the top of the skull. Prox1-GFP-negative/LYVE-1-positive tissue-localized macrophages had invaded the meninges and are mainly associated with the sinuses. (B, E) At P13, Prox1-GFP/LYVE-1-positive lymphatics are visible along the TS at top of the skull (arrow). (C, F) By P16, lymphatics extending along the TS reach the SSS (C, arrowhead) through the COS (C, arrow). The boxed regions in (A–C) are magnified in (D–F). The boxed region in (F) is magnified in (G–H), with staining using different antibodies. (G–G′) Near the TS at P16, developing Prox1-GFP-positive vessels (arrows) and cell clusters (arrowheads) are stained by Prox1 antibody staining. Note that there is some non-specific Prox1 antibody staining (open arrows). (H-H′) Near the TS at P16, extending Prox1-GFP-positive vessels (arrows) and cell clusters are also Podoplanin-positive. (I-I″) Lymphatic vessels in P6 ear skin are already established (I-I″, arrows), indicating that meningeal

lymphatic vessels develop at a delayed developmental time point. Open arrowheads indicate LYVE-1-positive tissue-localized macrophages. Scale = 1mm in (A–C) and 100 μm in (G–I, G′-I″).

Author Manuscript Author Manuscript Author Manuscript Author Manuscript

Author Manuscript Author Manuscript Author Manuscript Author Manuscript

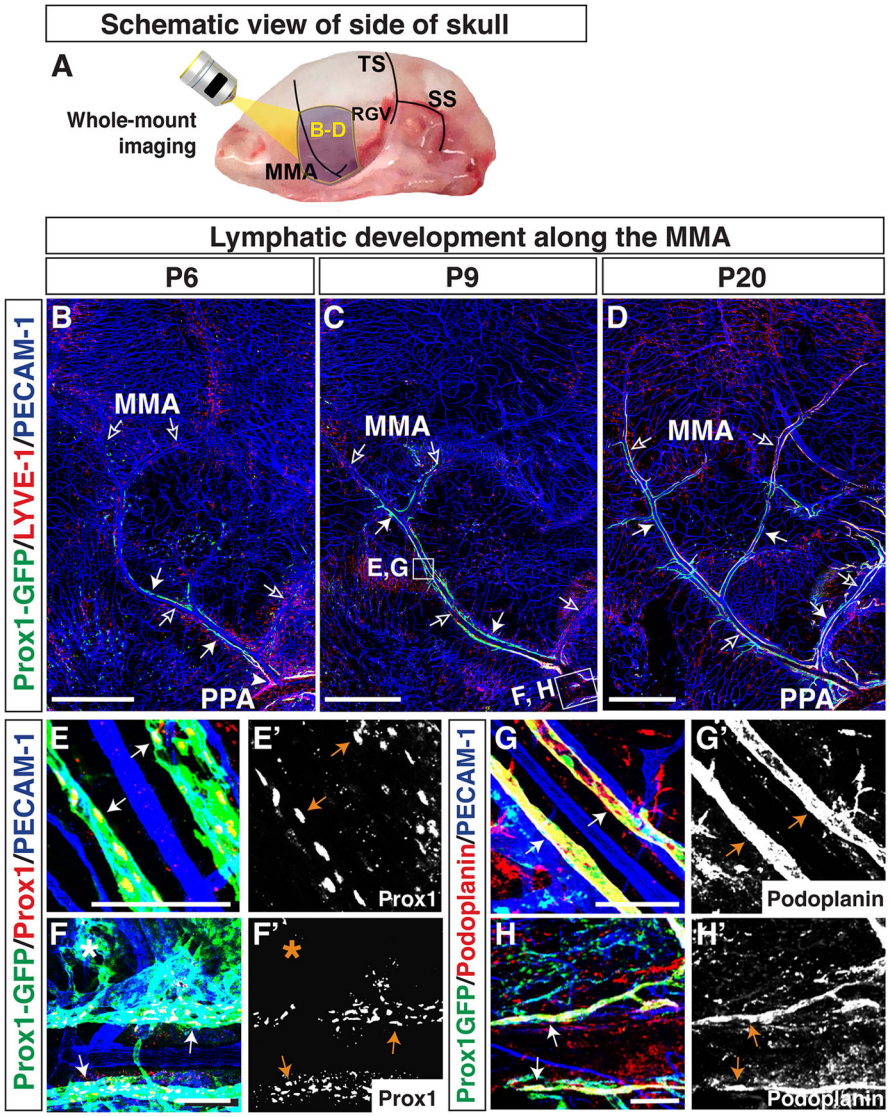

Figure 4.

Lymphatics on the side of the skull extend along the MMA from the pterygopalatine artery (PPA) towards the top of the skull. (A) Schematic of blood vessels in the dura mater at the side of the skull. The MMA, TS, retroglenoid vein (RGV), and sigmoid sinus (SS) are shown. The purple areas around the MMA are analyzed at different developmental time points as shown in (B–D), and the multiple open arrows in (B–D) indicate the MMA and its branches. (B) At P6, Prox1-GFP-positive/LYVE-1-weak lymphatic vessels (arrows) are distributed along the base of the MMA (open arrows), connecting with the PPA (arrowhead). (C) By P9, Prox1-GFP-positive/LYVE-1-weak lymphatic vessels (arrows) have extended along the MMA and one of its branches towards the top of the skull. (D) At P20, the Prox1-GFP-positive lymphatic vessels (arrows) have extended along several branches of the MMA, and most Prox1-GFP positive lymphatic vessels have enhanced LYVE-1 expression. The lymphatic vessels at the base of the MMA connect with Prox1-GFP/LYVE-1-double positive lymphatics along the PPA, which passes through the base of the skull. The boxed regions in

Author Manuscript Author Manuscript Author Manuscript Author Manuscript

(C) are magnified in (E–H), with staining using different antibodies. (E–F′) At P9, Prox1-GFP-positive lymphatic vessels along the MMA and PPA are labeled by Prox1 antibody staining. Some of the Prox1-GFP-positive vessel area (asterisk) is not stained with Prox1 antibody. (G–H′) At P9, Prox1-GFP-positive lymphatic vessels along the MMA and PPA are also positive for Podoplanin. Scale = 1mm in (B–D) and 100 μm in (E–H′).

Author Manuscript Author Manuscript Author Manuscript Author Manuscript

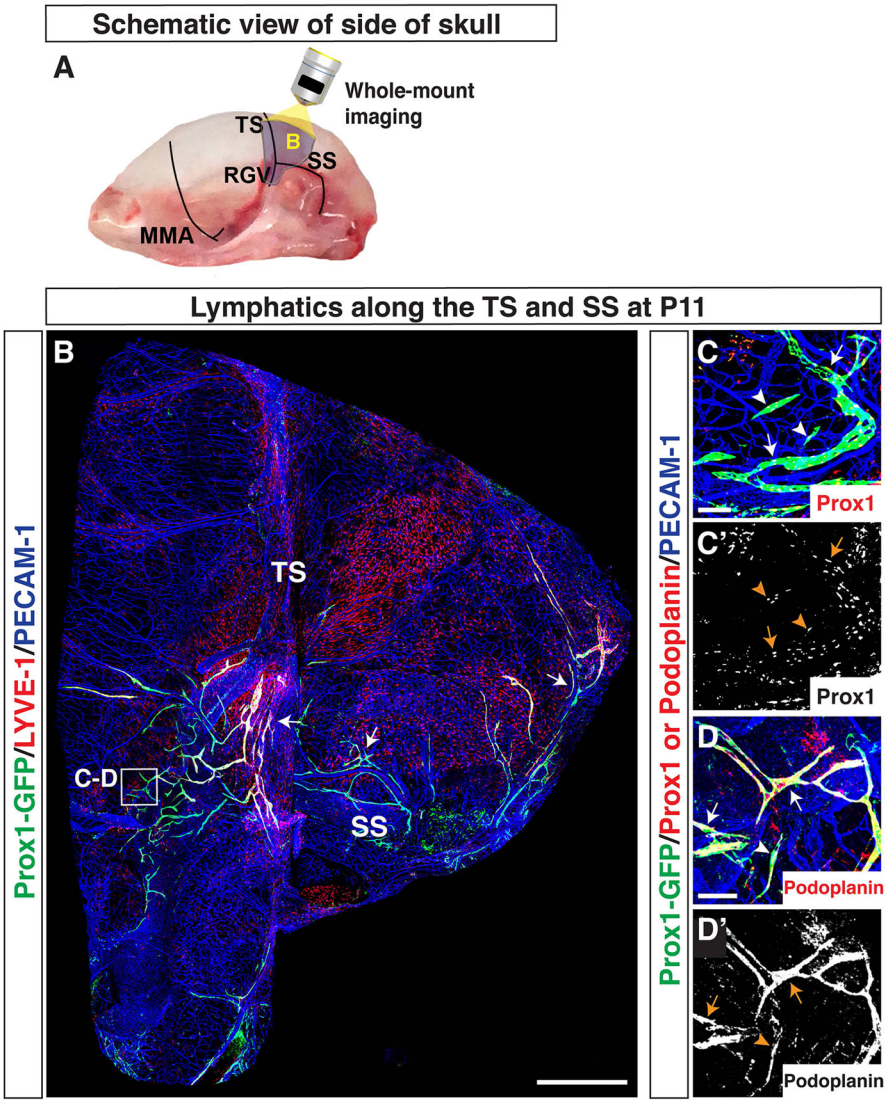

Figure 5.

Lymphatics on the side of the skull extend along the TS and SS. (A) Schematic of blood vessels in the dura mater at the side of the skull. The MMA, TS, RGV, and SS are shown. The purple area around the TS and SS is analyzed as shown in (B). (B) Developing Prox1-GFP-positive/LYVE-1-weak lymphatic vessels (arrow) extend from the base of the TS. Prox1-GFP-positive/LYVE-1-weak lymphatic vessels (arrow) along the SS extend to the base of the TS. Lymphatics associated with the SS also branch out over the cerebellum. The boxed region in (B) is magnified in (C–D), with staining using different antibodies. (C–D′) At the base of the TS, extensions of existing Prox1-GFP-positive vessels (arrows) and Prox1-GFP-positive cell clusters (arrowheads) are immunostained with antibodies to Prox1 (C-C′) and Podoplanin (D-D′). Scale = 1mm in (B) and 100 μm in (C–D′).

Author Manuscript Author Manuscript Author Manuscript Author Manuscript

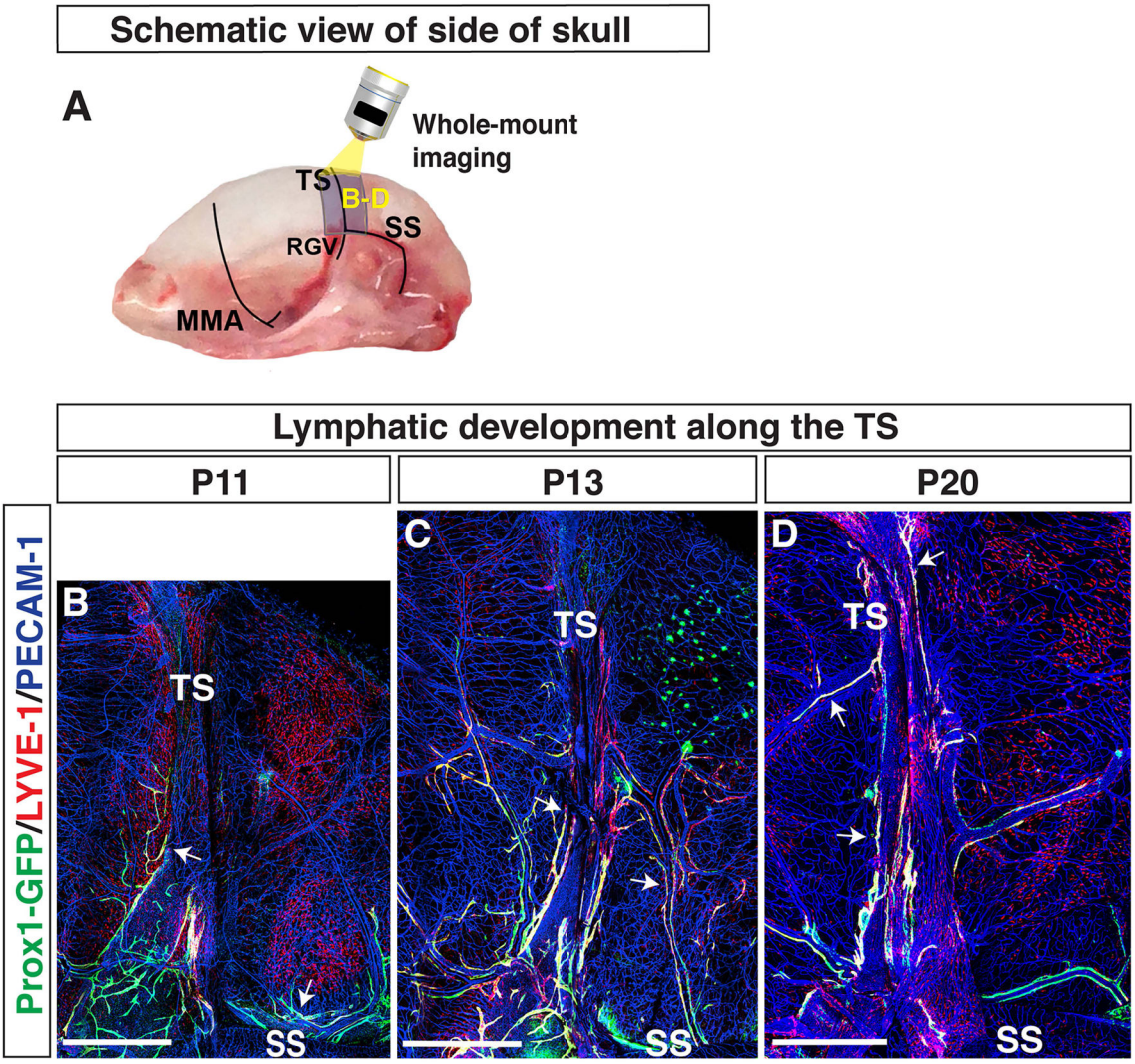

Figure 6.

Lymphatics on the side of the skull extend along the TS towards the top of the skull. (A) Schematic of blood vessels in the dura mater at the side of the skull. The MMA, TS, RGV, and SS are shown. The purple area around the TS is analyzed at different developmental time points as shown in (B–D), and the multiple open arrows in (B–D) indicate the TS and SS. (B) At P11, Prox1-GFP-positive/LYVE-1-weak lymphatic vessels exist along the SS and at the base of the TS (arrows). (C) At P13, Prox1-GFP/LYVE-1-double positive lymphatic vessels along the TS (arrows) extend towards the top of the skull. Prox1-GFP/LYVE-1-double positive lymphatic vessels from the SS extend upwards and connect with the lymphatic vessels along the TS. (C) At P20, Prox1-GFP/LYVE-1-double positive lymphatic vessels exist along the entire length of the TS. Scale = 1mm.

Author Manuscript Author Manuscript Author Manuscript Author Manuscript

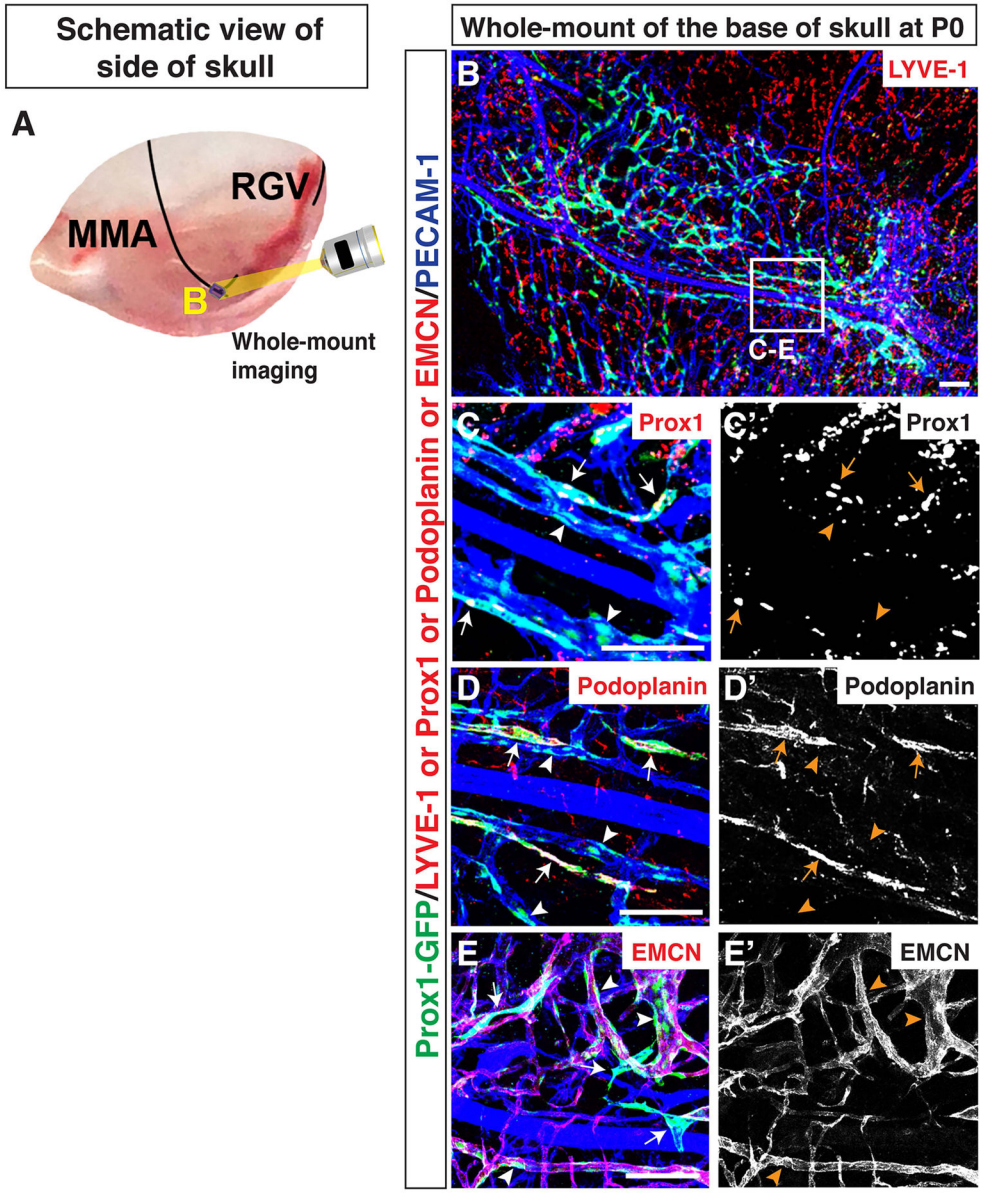

Figure 7.

Lymphatics along the MMA originate by P0. (A) Schematic of blood vessels in the dura mater at the side of the skull. The MMA and RGV are shown. The small purple region at the base of the MMA is analyzed as shown in B. (B) The PECAM-1 positive vascular plexus acquires Prox1-GFP expression around the base of the MMA. The boxed region in (B) is magnified in (C–E), with staining using different antibodies. (C–D′) Developing Prox1-GFP-positive lymphatics along the MMA are marked by immunostaining with antibodies to Prox1 (C-C′, arrows) and Podoplanin (D-D′, arrows). The majority of PECAM-1-positive capillaries near the MMA are positive for Prox1-GFP but negative for Prox1 and Podoplanin (C-C′, D-D′, arrowheads). (E-E′) There are two distinct Prox1-GFP-positive vessel populations: one Prox1-GFP-positive population that is not co-localized with a venous and

capillary endothelial cell marker EMCN (arrows), and one that is Prox1-GFP/EMCN-double positive (arrowheads). Scale = 1mm in (B) and and 100 μm in (C–E″).

Author Manuscript Author Manuscript Author Manuscript Author Manuscript

Author Manuscript Author Manuscript Author Manuscript Author Manuscript

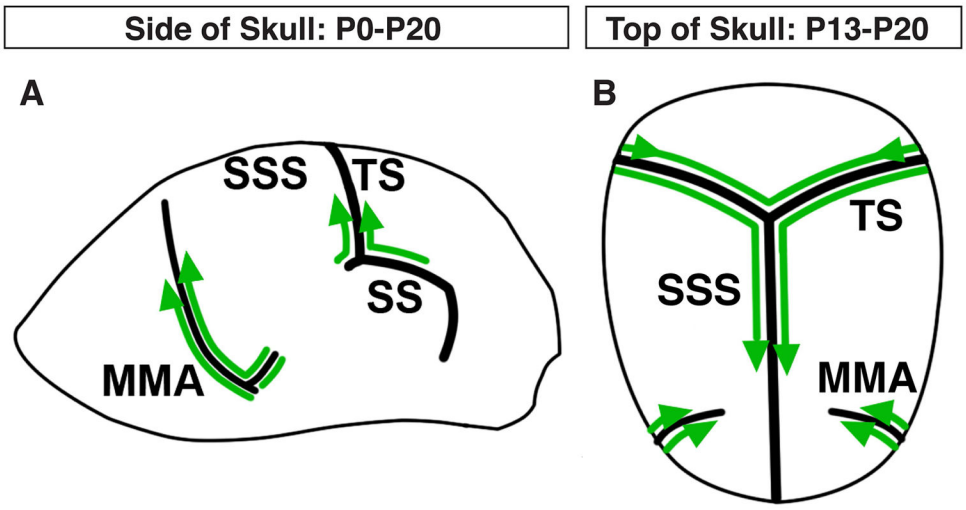

Figure 8.

Summary of postnatal meningeal lymphatic development. (A) Between P0–P13, lymphatics extend from the base of the MMA, the SS, and the base of the TS towards the top of the skull. (B) Between P13–P20, lymphatics along the TS reach the SSS and extend along the SSS towards the olfactory bulb. Lymphatics along the MMA also extend towards the SSS, but terminate before reaching the SSS.

Author Manuscript Author Manuscript Author Manuscript Author Manuscript

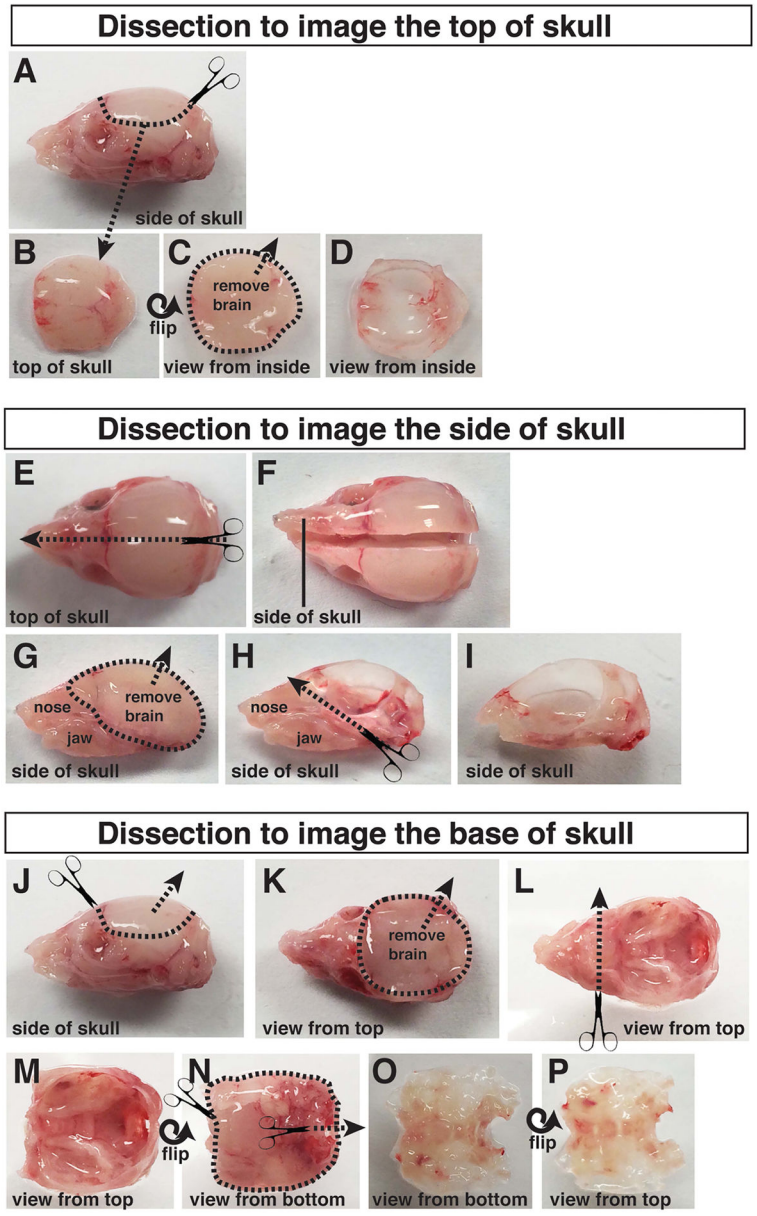

Figure 9.

Dissection of the P6 skull. (A–D) Top of skull dissection. (A–B) The top of the skull, with the brain still inside, is cut off and submerged in ice-cold PBS. (C–D) The brain is gently removed from the top of the skull. (E–I) Side of skull dissection. (E–F) The skull is cut in half sagittally. (G) The halved skull, with attached nose and jaws, is submerged in ice-cold PBS. The brain is gently removed from the skull. (H–I) The nose and jaws are trimmed away, along with any muscle, fat, and connective tissue attached to the outside of the skull. (J–P) Dissection of the base of the skull. (J–K) The top of the skull is cut off, and the brain is gently removed from the base of the skull. (K–L) The nose and eye sockets are cut away and

Author Manuscript Author Manuscript Author Manuscript Author Manuscript

the skull is flipped over to expose the underside of the face and jaw. (M–P) The lower jaw, fat, muscle, and connective tissue are trimmed off the base of the skull.

Author Manuscript

Author Manuscript

Author Manuscript

Author Manuscript

Table 1

Primary antibodies for whole-mount tissues and sections

Name	Species	Company	Conc.
GFP	Chicken polyclonal	Abcam #ab13970	1:300
	Rabbit polyclonal	Thermo Fisher Scientific #A11122	1:300
Prox1	Rabbit polyclonal	Millipore #AB5475	1:250
LYVE-1	Rabbit polyclonal	Abcam #ab14917	1:500
	Rat monoclonal	MBL #D225–3	1:500
Podoplanin	Syrian hamster monoclonal	DSHB 8.1.1	1:200
PECAM-1	Rat monoclonal	BD Pharmingen #553369	1:300
	Armenian hamster monoclonal	Millipore #MAB1398Z	1:200
EMCN	Rabbit polyclonal	Santa cruz #sc-65495	1:300
F4/80	Rat monoclonal	Bio-Rad #MCA497	1:50
CD206	Rabbit polyclonal	Abcam #ab 64693	1:400